Optica Applicata, Vol. XLII, No. 4, 2012
DOI: 10.5277/oa120420

Active phase-setting twin-frequency grating for 3D shape measurement based on an absolute phase unwrapping algorithm

ZHENFEN HUANG, YIPING CAO*, AIPING ZHAI, YANG LI, DELIANG CHEN

Opto-Electronics Department, Sichuan University, Chengdu, 610064, China

*Corresponding author: ypcao@scu.edu.cn

An active phase-setting twin-frequency grating based on an absolute phase unwrapping algorithm is proposed to measure the object with a complex shape. Two sinusoidal components with a spacial period ratio are combined into a twin-frequency grating, and two different initial phases are preset in two sinusoidal components, one of which is constant in a low-frequency component and the other is related to the ratio of two periods in a high-frequency component. Using the active phase-setting twin-frequency grating, two wrapped phases can be obtained from nine frames of distorted patterns by a regular phase shifting. Thus, the high-quality wrapped phase of a high-frequency component can be unwrapped by using an absolute phase unwrapping algorithm. Compared with a previous study based on a non-integral twin-frequency grating, the proposed grating needs a less number of patterns and the absolute phase unwrapping algorithm is easier to implement, so the proposed method is time-saving. The experimental results demonstrate that these achievements saved 90 percent of time approximately.

Keywords: 3D shape measurement, active phase-setting twin-frequency grating, absolute phase unwrapping algorithm.

1. Introduction

3D shape measurement is very important in machine vision, solid modeling, industrial auto-measuring, *etc*. [1–3]. Phase-measuring profilometry (PMP) [4], a typical 3D sensing technique with structured illumination, is notable for its systemic simplicity, full--field measurement capacity, high accuracy, and low environmental vulnerability. However, in traditional PMP, the projected structured light pattern is often a single frequency sinusoidal grating. The phase unwrapping process is path-dependent and measurement error is accumulative. It is not suitable for abrupt object surface measurement.

In order to solve the problems above, many methods using a path-independent phase unwrapping algorithm have been proposed [5–13]. For example, HUNTLEY and SALDNER [6] have proposed the temporal phase unwrapping method, which can restore the shape of an object with large height discontinuities. But, it needs too many gratings to achieve high-speed shape measurement. ZHAO *et al*. [8] have developed a significantly simple algorithm to measure the tested object twice with two sets of different single frequency sinusoidal gratings. Correct phase values can be obtained in the presence of discontinuities, but more manual interception to change the grating has a substantial influence on the automatic phase unwrapping. LI *et al*. [9] have presented a two-frequency grating in which the high frequency is N ($N \geq 3$) times greater than the low frequency. It is possible to unwrap the high-frequency phase with reference to the low-frequency phase. But low-frequency phase unwrapping is path-dependent, the phase unwrapping error can propagate in the high-frequency phase when shadow and speckle noise occur in the low-frequency phase. Both LIU *et al*. [10] and WANG *et al*. [11] are embedding a reference unit frequency signal into the projection patterns of the traditional phase-measuring-profilometry that does not use extra patterns. The proposed method is encouraging because of its capability of being put into the real-time 3D reconstruction. However, the reference frequency signal is sensitive to ambient light. Thus, our previous work [12] presented a non-integral twin-frequency grating (NITFG) for measuring discontinuous objects. By using an absolute phase unwrapping algorithm which is path-independent, phase errors were constrained within the high-noise regions. However, changing sixteen patterns is time--consuming, and the absolute phase unwrapping algorithm finding the right integers to match the equation for calculating the pattern order is intricate.

In this paper, by changing the period ratio of two sinusoidal components in a twin--frequency grating, an improved twin-frequency grating involving nine patterns is proposed. The new twin-frequency grating is also composed of two sinusoidal components, and the quotient of two periods of two components is not an integer. Comparing with NITFG, two initial phases are preset to the two sinusoidal components of the twin-frequency grating definitely. Otherwise, since there exists a fixed relationship between two wrapped phases, an absolute phase unwrapping method of a one-shot operation, a pixel-to-pixel phase unwrapping technique, is educed. The experimental results show that this new method, which combines a smaller number of patterns and the absolute phase unwrapping algorithm, can effectively maintain the accuracy of the measurement and retrieve the nature phase of the tested objects under the condition of a steep-shape speedily. Compared with the measuring time of 16.762 seconds using NITFG for 768×768 image sizes, we can restore the 3D shape of an object using an improved twin-frequency grating in 1.647 second. The new method is 10 times faster than the reported study based on NITFG. Applying the proposed method to various fields, such as the inspection of industrial products, the health monitoring of transportation systems or concrete structures, a 3D surface digitizing is expected.

2. Profilometry using non-integral twin-frequency grating projection

Here we briefly review the theory of NITFG (non-integral twin-frequency grating) [12]. The light intensity of NITFG obtained by CCD at pixel (x^c, y^c) is expressed as:

$$I^c(x^c, y^c) = A^c(x^c, y^c) + B_1^c(x^c, y^c)\cos\left[\frac{2\pi}{p_1}\gamma + \phi_1(x^c, y^c)\right] + \\ + B_2^c(x^c, y^c)\cos\left[\frac{2\pi}{p_2}\gamma + \phi_2(x^c, y^c)\right] \tag{1}$$

Intensity is varying along the x-axis. Where A^c is the background intensity, B_1^c and B_2^c represent the fringe contrast of the high-frequency component and the low-frequency component, respectively; γ is the phase step interval, p_1 and p_2 are the periods of the high-frequency component and the low-frequency component in captured patterns, and the relationship of two periods must be satisfied with certain condition for obtaining unwrapped phase uniquely;

$$p_1 : p_2 = 4:(4m + 1), \quad m = 1, 2, 3, \ldots \tag{2}$$

where m is the arbitrary integer; γ increases at the phase step of $p_2/4$. Therefore, sixteen images can be taken by CCD and two wrapped phases ϕ_1 and ϕ_2 can be retrieved simultaneously from the distorted patterns.

By introducing two wrapped phases, an intermediate S that represents the inherent relation of two wrapped phases is defined:

$$S(x^c, y^c) = (4m + 1)\frac{\phi_2(x^c, y^c)}{2\pi} - 4\frac{\phi_1(x^c, y^c)}{2\pi} \tag{3}$$

According to the absolute phase unwrapping algorithm proposed by HUANG *et al.*, the pattern order n_1 can be calculated with the following equation:

$$n_1(x^c, y^c) = \frac{(4m + 1)n'(x^c, y^c) + S(x^c, y^c)}{4} \\ \text{when } \left\{\text{mod}\left[(4m + 1)n'(x^c, y^c) + S(x^c, y^c), 4\right]\right\} = 0, \quad 0 \le n' \le (4m + 1) \tag{4}$$

where mod( ) denotes the remainder operator, n' is the integer that makes n_1 equal to an integer, and its values are taking four successive integers in the range of $0-(4m + 1)$.

By using Eq. (4), n_1 will take $(4m + 1)$ successive integer. Ultimately, the vertical dynamic range of an unwrapped phase is obtained to $2\pi(4m + 1)$.

3. New 3D shape measurement theorem

3.1. Active phase-setting twin-frequency grating

The layout of our structured light system for 3D shape measurement is shown in Fig. 1. The gratings generated by computer are sent to DLP projector and projected on the tested object sequentially. At the same time, a CCD synchronized with the projector is used to capture the reflected fringe images.

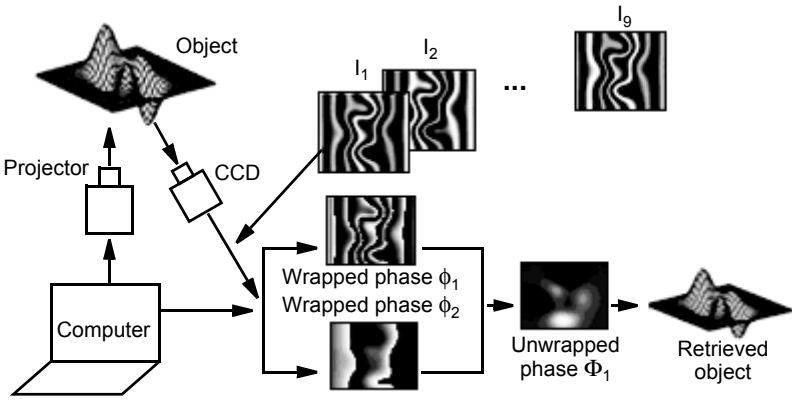

Fig. 1. Schematic diagram of the twin-frequency grating measurement system.

The light intensity I^p of an active phase-setting twin-frequency grating (APSTFG) for a pixel (x^p, y^p) in a projector can be expressed as:

$$I^p(x^p, y^p) = A^p(x^p, y^p) + B_1^p(x^p, y^p)\cos\left[\frac{2\pi}{P_1}\gamma + \frac{2\pi x^p}{P_1} + \varphi_1\right] + \\ + B_2^p(x^p, y^p)\cos\left[\frac{2\pi}{P_2}\gamma + \frac{2\pi x^p}{P_2} + \varphi_2\right] \tag{5}$$

where A^p, B_1^p and B_2^p are certain constants to make value of I^p between 0 and 255 for a 8-bit color depth projector. As mentioned above, the relationship of two periods in NITFG is satisfied with Eq. (2). Therefore, sixteen frames of patterns will be projected to measure objects. In order to select minimum frames of the projected grating, the relationship of two periods P_1 and P_2 in APSTFG is defined as:

$$P_1{:}P_2 = 3{:}(3m + 1), \quad m = 1, 2, 3, \ldots \tag{6}$$

when m is selected, the ratio of the periods of two sinusoidal components can be set. The φ_1 and φ_2 represent the initial phases of the high-frequency component and

the low-frequency component, which can make the two sinusoidal components shift along the *x*-axis. The values of φ_1 and φ_2 are given in the following formulas:

$$\varphi_1 = \frac{2\pi\Delta x_1}{P_1}, \qquad \varphi_2 = \frac{2\pi\Delta x_2}{P_2} \tag{7}$$

where Δx_1 and Δx_2 are the shift length of grating for the high-frequency component and the low-frequency component, respectively. In traditional grating generation technology, the values of the initial phase φ_1 and φ_2 are zeros, corresponding to $\Delta x_1 = \Delta x_2 = 0$. Figure 2**a** illustrates the first grating at $m = 8$ ($P_1{:}P_2 = 3{:}25$) and $\varphi_1 = \varphi_2 = 0$.

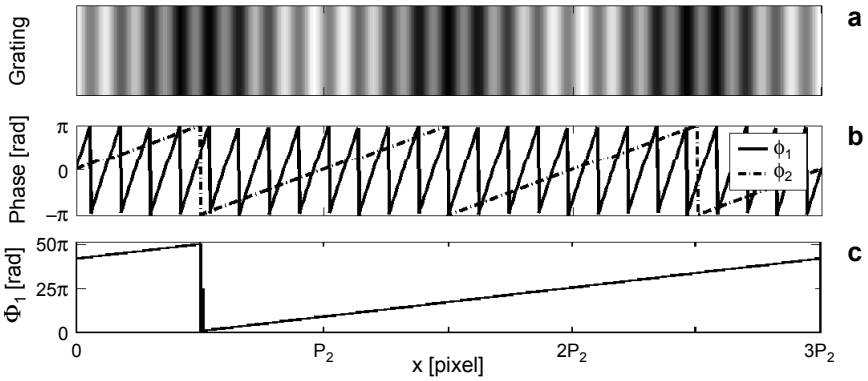

Fig. 2. Example of APSTFG at $m = 8$ and $\varphi_1 = \varphi_2 = 0$. Intensity image (**a**). Distributions of wrapped phase ϕ_1 and ϕ_2 (**b**). Distribution of unwrapped phase Φ_1 (**c**).

In new projected grating, γ increases at a regular interval $P_2/3$ of to match the new ratio of P_1 and P_2. Thus, the distorted patterns I_j^c obtained by CCD camera are expressed as:

$$I_j^c(x^c, y^c) = A^c(x^c, y^c) + B_1^c(x^c, y^c)\cos\left[2\pi\frac{p_2}{3p_1}(j-1) + \phi_1(x^c, y^c)\right] + \\ + B_2^c(x^c, y^c)\cos\left[\frac{2\pi}{3}(j-1) + \phi_2(x^c, y^c)\right] \tag{8}$$

where j is the number of acquired patterns ($j = 1, 2, \ldots, 9$). The relationship of two periods p_1 and p_2 captured by CCD is also satisfied with Eq. (6). The following equation can be obtained from Eq. (6):

$$2\pi\frac{p_2}{p_1} = 2\pi\frac{3m+1}{3} = 2\pi m + \frac{2\pi}{3} \tag{9}$$

Substituting Eq. (9) into Eq. (8), the captured nine patterns are written as follows:

$$I_1^c = A^c + B_1^c \cos(\phi_1) + B_2^c \cos(\phi_2) \tag{10}$$

$$I_2^c = A^c + B_1^c \cos\left(2\pi \frac{p_2}{3p_1} + \phi_1\right) + B_2^c \cos\left(2\pi \frac{p_2}{3p_1} + \phi_2\right) \tag{11}$$

$$I_3^c = A^c + B_1^c \cos\left(2\pi \frac{2p_2}{3p_1} + \phi_1\right) + B_2^c \cos\left(2\pi \frac{2p_2}{3p_1} + \phi_2\right) \tag{12}$$

$$I_4^c = A^c + B_1^c \cos\left(\frac{2\pi}{3} + \phi_1\right) + B_2^c \cos(\phi_2) \tag{13}$$

$$I_5^c = A^c + B_1^c \cos\left(\frac{2\pi}{3} + 2\pi \frac{p_2}{3p_1} + \phi_1\right) + B_2^c \cos\left(\frac{2\pi}{3} + \phi_2\right) \tag{14}$$

$$I_6^c = A^c + B_1^c \cos\left(\frac{2\pi}{3} + 2\pi \frac{2p_2}{3p_1} + \phi_1\right) + B_2^c \cos\left(\frac{4\pi}{3} + \phi_2\right) \tag{15}$$

$$I_7^c = A^c + B_2^c \cos\left(\frac{4\pi}{3} + \phi_1\right) + B_2^c \cos(\phi_2) \tag{16}$$

$$I_8^c = A^c + B_1^c \cos\left(\frac{4\pi}{3} + 2\pi \frac{p_2}{3p_1} + \phi_1\right) + B_2^c \cos\left(\frac{2\pi}{3} + \phi_2\right) \tag{17}$$

$$I_9^c = A^c + B_1^c \cos\left(\frac{4\pi}{3} + 2\pi \frac{2p_2}{3p_1} + \phi_1\right) + B_2^c \cos\left(\frac{4\pi}{3} + \phi_2\right) \tag{18}$$

In Equations (10)–(12), the low-frequency terms are equivalent and the high-frequency terms increase at the phase stepping of $2\pi/3$. Therefore, adopting the *N*-phase-shifts [4] algorithm, ϕ_1 of high-frequency can be retrieved firstly

$$\phi_1 = \operatorname{atan}\left[\frac{\sqrt{3}(I_7^c - I_4^c)}{2I_1^c - I_4^c - I_7^c}\right] = \delta_1 \tag{19}$$

Using the same manner, the following equations are also obtained:

$$\phi_1 + 2\pi \frac{p_2}{3p_1} = \operatorname{atan}\left[\frac{\sqrt{3}(I_8^c - I_5^c)}{2I_2^c - I_5^c - I_8^c}\right] = \delta_2 \tag{20a}$$

$$\phi_1 + 2\pi \frac{2p_2}{3p_1} = \operatorname{atan}\left[\frac{\sqrt{3}(I_9^c - I_6^c)}{2I_3^c - I_6^c - I_9^c}\right] = \delta_3 \tag{20b}$$

Then, substituting Eqs. (19) and (20) into Eqs. (10)–(18), B_1^c can be obtained from those nine equations:

$$B_1^c = \frac{2\sum_{j=1}^{3} I_j^c - \sum_{j=4}^{9} I_j^c}{2\sum_{j=1}^{3}\cos(\delta_j) - \sum_{j=1}^{3}\cos\left(\delta_j + \frac{2\pi}{3}\right) - \sum_{j=1}^{3}\cos\left(\delta_j + \frac{4\pi}{3}\right)} \tag{21}$$

Moreover, Eqs. (10)–(12) can be simplified by B_1^c and a new variable I' is introduced:

$$I_1' = I_1^c - B_1^c\cos(\delta_1) = A^c + B_2^c\cos(\phi_2) \tag{22a}$$

$$I_2' = I_2^c - B_1^c\cos(\delta_2) = A^c + B_2^c\cos\left(\frac{2\pi}{3} + \phi_2\right) \tag{22b}$$

$$I_3' = I_3^c - B_1^c\cos(\delta_3) = A^c + B_2^c\cos\left(\frac{4\pi}{3} + \phi_2\right) \tag{22c}$$

Thus, ϕ_2 can be calculated easily:

$$\phi_2 = \operatorname{atan}\left(\frac{\sqrt{3}\,I_3' - I_2'}{2I_1' - I_2' - I_3'}\right) \tag{23}$$

Figure 2**b** presents the cross-sections of ϕ_1 and ϕ_2 with a solid-line and dotted-line, respectively, when the initial phases φ_1 and φ_2 of two sinusoidal components are zeros. It can be seen that the values of ϕ_1 and ϕ_2 are equal to zeros at $x = 0$.

3.2. Absolute phase unwrapping algorithm

In order to recover the absolute phase, phase unwrapping will encounter ambiguity to distinguish the pattern order. Many phase-unwrapping algorithms have been developed [15–19] for removing the phase jumps. We have proposed an absolute phase unwrapping algorithm [12]. However, it is intricate and time-consuming to find the right integers of n' to satisfy the conditional equation in Eq. (4). Thus, for reducing the computational complexity, the absolute phase unwrapping algorithm is improved.

The relationship between the wrapped phase and the unwrapped phase can be expressed independently as:

$$\Phi_1 = 2n_1\pi + \phi_1, \qquad \Phi_2 = 2n_2\pi + \phi_2 \tag{24}$$

where, Φ_1 and Φ_2 are the unwrapped phases of ϕ_1 and ϕ_2, respectively, n_1 and n_2 are unknown integers. Otherwise, the relationship between Φ_1 and Φ_2 corresponding to different periods can be also expressed as:

$$\Phi_1 = \frac{p_2}{p_1}\Phi_2 = \frac{3m+1}{3}\Phi_2 \tag{25}$$

Thus, S can be obtained from Eq. (24) and Eq. (25),

$$(3m+1)\frac{\phi_2}{2\pi} - 3\frac{\phi_1}{2\pi} = \frac{(3m+1)\Phi_2 - 3\Phi_1 - 2\pi\left[(4m+1)n_2 - 4n_1\right]}{2\pi} =$$

$$= 4n_1 - (4m+1)n_2 = S \tag{26}$$

It can be noted that S is unique to the components of n_1 and n_2, so S must be an integer. In practical measurement, the calculated value S always contains a decimal part, so it needs to be rounded to the nearest integer. Thus, a new absolute phase unwrapping algorithm is presented as,

$$n_1 = \frac{S + (3m+1)(2 - \mathrm{mod}(S, 3)) + 3\left[\frac{m}{2}\right] + 1}{3} \tag{27}$$

where mod( ) also is the operator of remainder, and [ ] is the operator of rounding down. The new absolute phase unwrapping algorithm can obtain the values of n_1 with a one-shot operation.

Figure 3 illustrates the detailed process of improved phase unwrapping algorithm when $m = 8$. Firstly, the wrapped phase ϕ_1 is multiplied by 3 and ϕ_2 is multiplied by 25, thus S can be obtained by Eq. (26). Secondly, by using Eq. (27), n_1 is obtained. Lastly, with the Eq. (24), the unwrapped phase Φ_1 is obtained, as shown in Fig. 2**c**.

3.3. Initial phases setting

From Fig. 2, it can be noted that the unwrapped phase Φ_1 is discontinuous at the point of $P_2/2$ when the initial phases of two sinusoidal components in the twin-frequency

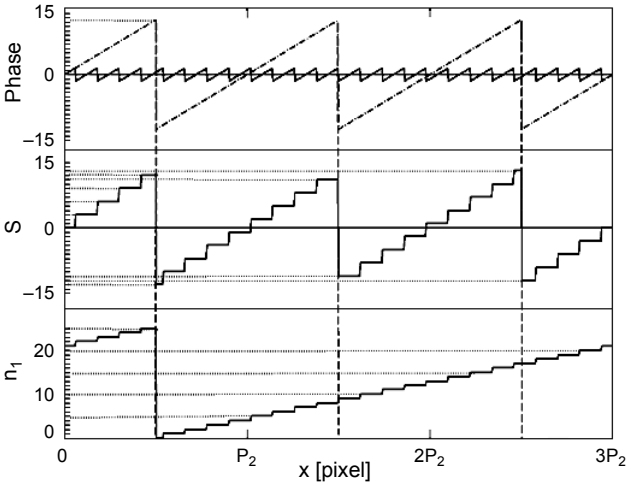

Fig. 3. The process of absolute phase unwrapping algorithm.

grating are zeros. This discontinuous point is coinciding with the first transition (from $3\pi/2$ to $-\pi/2$) of ϕ_2, so it does not change with m. In our previous work [12], the values of two initial phases in the two sinusoidal components of NITFG have not been stated. Therefore, in order to ensure that Φ_1 can be unwrapped completely in the field of $3P_2$, where $3P_2$ is the least common multiple of P_1 and P_2, both values φ_1 and φ_2 of two sinusoidal components are specified as the following formulas to shift the grating of $P_2/2$ along the x-axis,

$$\varphi_1 = \frac{2\pi\Delta x_1}{P_1} = \frac{2\pi(P_2/2)}{P_1} \tag{28a}$$

$$\varphi_2 = \frac{2\pi\Delta x_2}{P_2} = \frac{2\pi(P_2/2)}{P_2} \tag{28b}$$

corresponding to $\Delta x_1 = \Delta x_2 = P_2/2$. Substituting Eq. (6) into Eq. (28), φ_1 and φ_2 can be obtained:

$$\begin{cases} \varphi_1 = \dfrac{1 + \mathrm{mod}(m, 2) \times 3}{3}\pi \\ \varphi_2 = \pi \end{cases} \tag{29}$$

Apparently, φ_1 will be set when m is selected.

Figure 4**a** shows the first frame of the APSTFG in the case of $m = 8$, $\varphi_1 = \pi/3$ and $\varphi_2 = \pi$. Using the phase generation algorithm from Eq. (19) to Eq. (23), the cross-sections of reference plane's wrapped phase ϕ_1 and ϕ_2 after two initial phases being preset

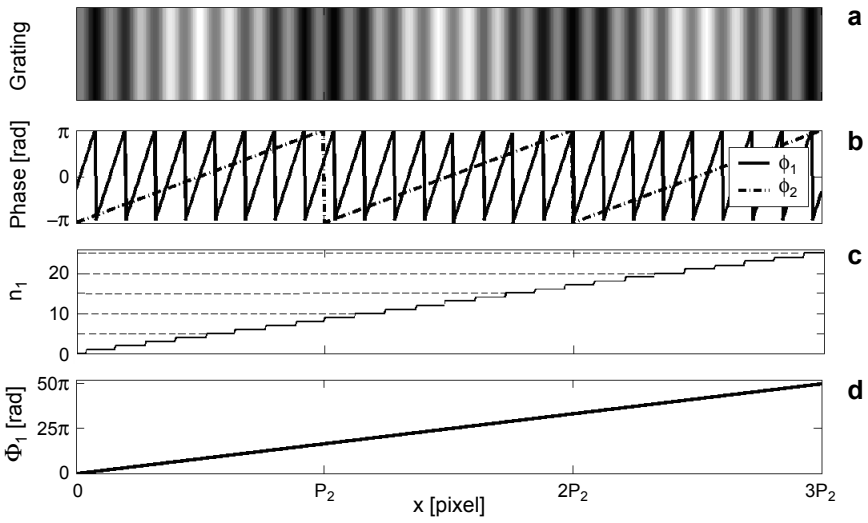

Fig. 4. Example of APSTFG at $m = 8$, $\varphi_1 = \pi/3$ and $\varphi_2 = \pi$. Intensity image (**a**). Distributions of wrapped phase ϕ_1 and ϕ_2 (**b**). Distribution of n_1 (**c**). Distribution of unwrapped phase Φ_1 (**d**).

are shown in Fig. 4**b**. Comparing to Figs. 2**a** and 2**b**, the twin-frequency grating and two wrapped phases are all shifted by $P_2/2$ along the x-axis successively. Using Eq. (27), n_1 is obtained in the range of 0–25, as shown in Fig. 4**c**. Lastly, the wrapped phase ϕ_1 is unwrapped completely in the field of $3P_2$ and Φ_1 distributed in the range of $0 \leq \Phi_1 \leq 50\pi$, as shown in Fig. 4**d**.

4. Experiment

In our experiment, the projector adopts HCP-75X with a frame rate of 120 fps and 1024×768 pixel resolution, and the imaging sensor adopts MTV1881EX with a frame rate of 6 fps at 80 ms exposure time and 1024×768 pixel resolution. Both the projector and the imaging sensor are controlled by in-house software written in C++ to achieve automatic measurement. As our processing unit, we use a ThinkPad E40 with an Intel Core i3 380M processor running at 2.53 GHz.

In order to test the performance of the proposed pattern scheme, the horizontal gratings are generated using Eq. (5) based on selecting the ratio of periods in Eq. (6) and presetting the initial phase in Eq. (29). The period of the high-frequency component will decrease with the increasing of m. When the number of pixels in a period of the high-frequency component captured by CCD is less than 4, which disobeys the sampling theorem [20], the phase unwrapping errors will occur. Otherwise, it would be too difficult to ensure an accurate measurement if the period of the high-frequency component is too large. We take $m = 8$ for example in the following experiment. Thus the periods p_1 and p_2 of APSTFG are about 14.2 mm and 118.3 mm in the reference plane, respectively.

At first, eight planes with the height step of 20 mm are measured for validating the measurement accuracy of the proposed method. Table 1 reports the maximum error (ME) and the standard deviation (SD) of tested planes. It can be found that the maximum error is 0.161 mm, which is 0.09% of the measurement height of 160 mm. And SD is below 0.053 mm at each plane.

Secondly, two isolated boxes with large discontinuities and locally different reflectivity are used for testing the performance of the proposed method. The first

T a b l e 1. Measurement accuracy of eight planes with new method.

Height of tested planes [mm]	ME [mm]	SD [mm]
20	0.099	0.043
40	0.142	0.048
60	0.125	0.052
80	0.114	0.035
100	0.151	0.043
120	0.142	0.053
140	0.135	0.051
160	0.161	0.047

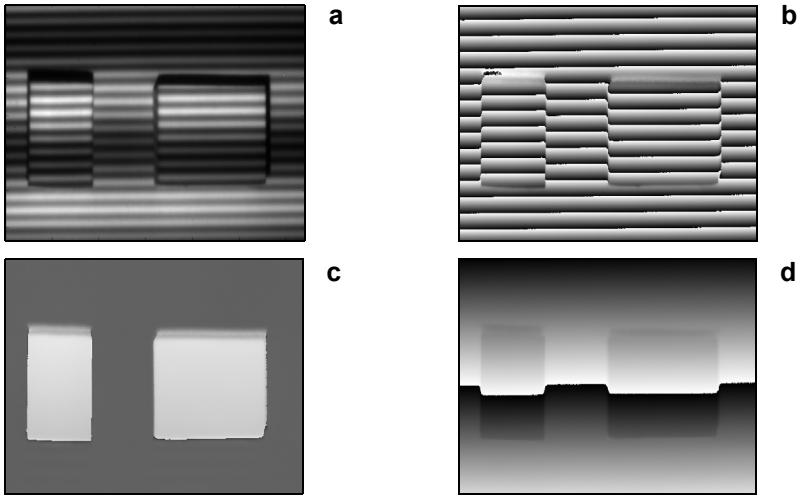

Fig. 5. Measurement results of two boxes. Distorted pattern (**a**), wrapped phase ϕ_1 (**b**), wrapped phase ϕ_2 (**c**), unwrapped phase Φ_1 (**d**).

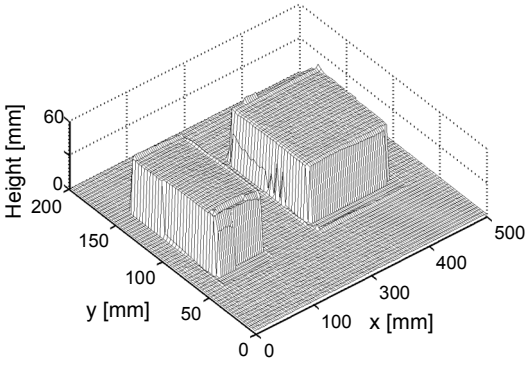

◀ Fig. 6. Reconstructed two isolated boxes.

frame of the nine distorted patterns is shown in Fig. 5**a**. With the patterns captured by CCD, the two wrapped phases solved from nine patterns are shown in Figs. 5**b** and 5**c**. Based on the absolute phase unwrapping algorithm, the unwrapped phase of the tested object obtained from the high-frequency phase is shown in Fig. 5**d**. The reconstructed 3D surfaces by the phase-to-height mapping [13] are shown in Fig. 6. It can be seen that the novel 3D sensing method can restore the isolated objects rightly. In addition, a face mask is also measured, as shown in Fig. 7. One of the distorted patterns is shown in Fig. 7**a**. The reconstructed 3D surface of the face mask is shown in Fig. 8. It shows that the complex surface object can also be restored successfully.

Lastly, for the purpose of comparing the measuring speed, the objects with different sizes are tested by using NITFG and APSFMG, which are based on the respective absolute phase unwrapping algorithm. Table 2 shows the total measuring time, including image acquisition and data processing (phase generation, phase unwrapping, and 3D reconstruction). It can be seen that total measuring time using NITFG is 6.769 s

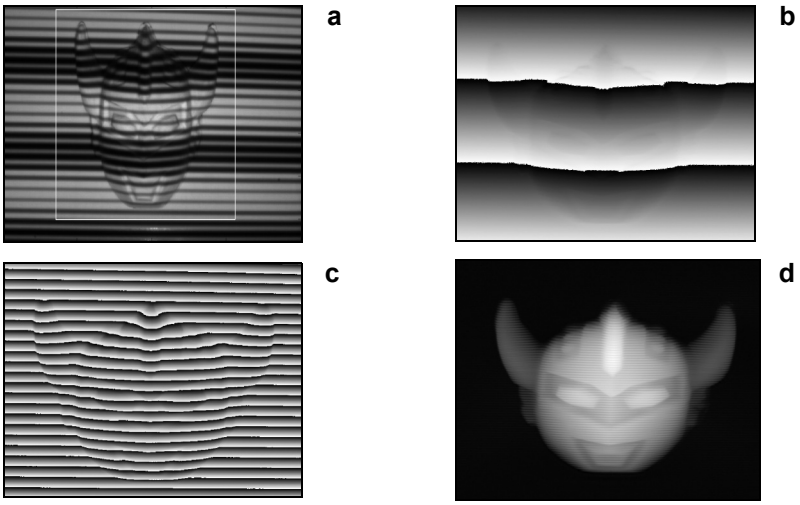

Fig. 7. Measurement of face mask. Distorted pattern of APSTFG (**a**), wrapped phase ϕ_1 (**b**), wrapped phase ϕ_2 (**c**), unwrapped phase Φ_1 (**d**).

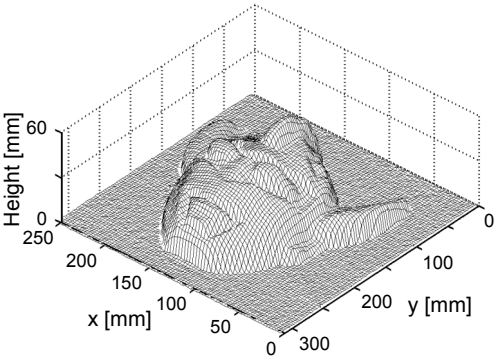

◀ Fig. 8. Reconstructed face mask.

for 512×512 image sizes, 16.762 s for 768×768 image sizes, and 23.989 s for 1024×768 image sizes, versus, using APSTFG, 1.571 s for 512×512 image sizes, 1.647 s for 768×768 image sizes, and 1.789 s for 1024×768 image sizes, which means that the 3D shape measurement method based on APSTFG is about 10 times faster than NITFG. The acquisition time of images, which is independent of an image size, is about 2.7 s for NITFG, versus, 1.5 s for APSTFG. Although the acquisition time decreases by using APSTFG, the response time of the imaging sensor is the main limiting factor of high-speed measuring. By using a faster imaging sensor, the acquisition time of images can be shortened. The processing time of data is increased with larger image sizes, because larger image sizes mean more summation, subtraction, and arcus tangens computations. The processing time of phase unwrapping, the main factor of data processing, decreases significantly, such as 0.114 s for APSTFG with

T a b l e 2. Measuring time for different image sizes with NITFG and APSTFG.

	NITFG			APSTFG		
Processing time(s)	512×512	768×768	1024×768	512×512	768×768	1024×768
Image acquisition	2.654	2.696	2.712	1.508	1.497	1.586
Phase generation	0.027	0.068	0.086	0.013	0.045	0.069
Phase unwrapping	3.831	13.98	21.17	0.042	0.086	0.114
3D reconstruction	0.009	0.018	0.021	0.008	0.019	0.020
Total processing	6.769	16.762	23.989	1.571	1.647	1.789

1024×768 image sizes, compared with 21.17 s for NITFG. With data for processing becoming larger, the new method has an excellent performance for promoting the speed of calculation.

5. Conclusions

The new optical sensing method based on an ASPTFG is put forward and investigated. The active phase-setting technology in which two different initial phases are preset in the twin-frequency grating is applied. By changing the period ratio of two sinusoidal components, the numbers of projected grating decrease. In addition, an improved absolute phase-unwrapping method is presented to reduce computation complexity. The experiments of eight planes show that the maximum of measurement error for the eight planes is 0.161 mm, which is 0.09% of the measurement height of 160 mm. The experimental data demonstrate the effectiveness of the proposed method in measuring the objects with a high and sharp profile. Furthermore, in contrast to previous studies of NITFG, the achievements in this paper demonstrated in Table 2 saved 90% of time approximately. In the future, this method will be a better choice for high-accuracy and real-time shape measurement.

Acknowledgements – This work is supported by 863 National Plan Foundation of China under grant No. 2007AA01Z333.

References

[1] CHEN F., BROWN G.M., SONG M., *Overview of three-dimensional shape measurement using optical methods*, Optical Engineering **39**(1), 2000, pp. 10–22.

[2] XIANYU SU, WENJING CHEN, *Fourier transform profilometry: a review*, Optics and Lasers in Engineering **35**(5), 2001, pp. 263–284.

[3] SRINIVASAN V., LIU H.C., HALIOUA M., *Automated phase-measuring profilometry: a phase mapping approach*, Applied Optics **24**(2), 1985, pp. 185–188.

[4] XIAN-YU SU, VON BALLY G., VUKICEVIC D., *Phase-stepping grating profilometry: utilization of intensity modulation analysis in complex objects evaluation*, Optics Communications **98**(1–3), 1993, pp. 141–150.

[5] GUSHOV V.I., SOLODKIN YU.N., *Automatic processing of fringe patterns in integer interferometers*, Optics and Lasers in Engineering **14**(4–5), 1991, pp. 311–324.
[6] HUNTLEY J.M., SALDNER H.O., *Temporal phase-unwrapping algorithm for automated interferogram analysis*, Applied Optics **32**(17), 1993, pp. 3047–3052.
[7] JINDONG TIAN, XIANG PENG, XIAOBO ZHAO, *A generalized temporal phase unwrapping algorithm for three-dimensional profilometry*, Optics and Lasers in Engineering **46**(4), 2008, pp. 336–342.
[8] HONG ZHAO, WENYI CHEN, YUSHAN TAN, *Phase-unwrapping algorithm for the measurement of three-dimensional object shapes*, Applied Optics **33**(20), 1994, pp. 4497–4500.
[9] JIE-LIN LI, HONG-JUN SU, XIAN-YU SU, *Two-frequency grating used in phase-measuring profilometry*, Applied Optics **36**(1), 1997, pp. 277–280.
[10] KAI LIU, YONGCHANG WANG, LAU D.L., QI HAO, HASSEBROOK L.G., *Dual-frequency pattern scheme for high-speed 3-D shape measurement*, Optics Express **18**(5), 2010, pp. 5229–5244.
[11] YONGCHANG WANG, KAI LIU, QI HAO, LAU D.L., HASSEBROOK L.G., *Period coded phase shifting strategy for real-time 3-D structured light illumination*, IEEE Transactions on Image Processing **20**(11), 2011, pp. 3001–3013.
[12] ZHENFEN HUANG, YIPING CAO, AIPING ZHAI, YUHANG HE, JUN KOU, *A novel 3D measuring method for discontinuous object by non-integral twin-frequency grating*, Optik – International Journal for Light and Electron Optics **123**(21), 2012, pp. 1915–1919.
[13] IKEDA Y., YONEYAMA S., FUJIGAKI M., MORIMOTO Y., *Absolute phase analysis method for three-dimensional surface profilometry using frequency-modulated grating*, Optical Engineering **42**(5), 2003, pp. 1249–1256.
[14] WANSONG LI, XIANYU SU, ZHONGBAO LIU, *Large-scale three-dimensional object measurement: a practical coordinate mapping and image data-patching method*, Applied Optics **40**(20), 2001, pp. 3326–3333.
[15] GHIGLIA D.C., ROMERO L.A., *Robust two-dimensional weighted and unweighted phase unwrapping that uses fast transforms and iterative methods*, Journal of the Optical Society of America A **11**(1), 1994, pp. 107–117.
[16] HONG ZHANG, HONGJUN SU, XIAN-YU SU, *Automatic phase unwrapping algorithm for reconstruction of three-dimensional objects*, Optics Letters **32**(21), 2007, pp. 3119–3121.
[17] STETSON K.A., WAHID J., GAUTHIER P., *Noise-immune phase unwrapping by use of calculated wrap regions*, Applied Optics **36**(20), 1997, pp. 4830–4838.
[18] JIN-JUNG CHYOU, SHEAN-JEN CHEN, YI-KUANG CHEN, *Two-dimensional phase unwrapping with a multichannel least-mean-square algorithm*, Applied Optics **43**(30), 2004, pp. 5655–5661.
[19] HONG ZHANG, HONGJUN SU, XIAN-YU SU, *Automatic phase unwrapping algorithm for reconstruction of three-dimensional objects*, Optics Letters **32**(21), 2007, pp. 3119–3121.
[20] SU X.Y., LI J.T., *Optical Information Processing*, 7th Edition, Science Press, Beijing 1999, p. 323, (in Chinese).

Received January 21, 2012
in revised form May 15, 2012